Opto-Electronic Advances

Original Article

2022, Vol. 5, No. 9

DOI: 10.29026/oea.2022.210065

0.35% THz pulse conversion efficiency achieved by Ti:sapphire femtosecond laser filamentation in argon at 1 kHz repetition rate

Zhiqiang Yu[1,2†], Nan Zhang[1,2†], Jianxin Wang[1,2], Zijie Dai[1,2], Cheng Gong[1,2], Lie Lin[1,3], Lanjun Guo[1,2] and Weiwei Liu[1,2*]

In this study, an optical setup for generating terahertz (THz) pulses through a two-color femtosecond laser filament was carefully designed to achieve a precise overlap of two-color laser pulses in space and time. β-barium borate (BBO), α-BBO, and a dual-wavelength plate were used to compensate the phase delay of the two-color lasers. Tilting of α-BBO could further realize the precise spatial overlap of the two beams by counteracting the walk-off effect. The maximum output THz pulse energy reached 21 μJ in argon gas when using a commercial Ti:sapphire laser with a pulse energy of 6 mJ at a 1 kHz repetition rate. The corresponding conversion efficiency exceeded 0.35%.

Keywords: femtosecond laser filaments; walk-off effect; conversion efficiency

Yu ZQ, Zhang N, Wang JX, Dai ZJ, Gong C et al. 0.35% THz pulse conversion efficiency achieved by Ti:sapphire femtosecond laser filamentation in argon at 1 kHz repetition rate. *Opto-Electron Adv* **5**, 210065 (2022).

Introduction

The availability of terahertz (THz) waves has enabled unprecedented research on the properties of matter[1]. To achieve further control over matter and light by using THz transients, the interaction of intense femtosecond lasers with nonlinear materials[2] has received considerable research interest. THz radiations with pulse energies of 436 μJ have been generated through optical rectification in lithium niobate (LN)[3] with an energy conversion efficiency of 0.77%. Recently, the output THz pulse energy was boosted to 1.4 mJ by pumping a large-area LN crystal (80 mm× 26.5 mm) with a 214 mJ Ti:sapphire laser pulse[4] and the energy conversion efficiency is 0.65%. Furthermore, when the organic crystals[5,6] are used, the THz energy conversion efficiency via the optical rectification can be up to 3%. On the other hand, the record-high THz pulse energy of 50 mJ was generated by a 60 J picosecond laser pulse irradiating a metal foil with an energy conversion efficiency of 0.08%[7]. The highest THz pulse energy conversion efficiency during the interaction between femtosecond laser and the metallic material was reported to reach ~1% using a 3 mJ laser interaction with a metal wire in a single-shot experiment[8].

Furthermore, THz pulse generation through a femtosecond laser interaction with gas plasma, i.e., femtosecond laser filamentation, has attracted broad attention in view of its damage-free and ultrabroad bandwidth[9–12]. A bandwidth as broad as 200 THz has also been demonstrated[13]. This technique is also considered as the only way to generate THz radiation remotely in atmosphere[1].

[1]Institute of Modern Optics, Nankai University, Tianjin 300350, China; [2]Tianjin Key Laboratory of Micro-scale Optical Information Science and Technology, Tianjin 300350, China; [3]Tianjin Key Laboratory of Optoelectronic Sensor and Sensing Network Technology, Tianjin 300350, China.
†These authors contributed equally to this work.
*Correspondence: WW Liu, E-mail: liuweiwei@nankai.edu.cn

Received: 16 May 2021; Accepted: 27 July 2021; Published online: 27 July 2022

However, the main challenge in this field lies in the significant enhancement of the output THz pulse energy[1]. The highest pulse energy was estimated to be 0.185 mJ, which is obtained by mixing infrared light with a central wavelength of 3.9 μm and its second harmonic (SH)[14]. The energy conversion efficiency is 2.36%. However, the restricted accessibility of the intense mid-infrared femtosecond laser system limits the extensive application of similar methods. Except for extending the pumping laser to long wavelengths[15], different approaches have been explored to increase the THz pulse energy, such as paralleling the polarizations of two-color laser pulses by a double-wavelength plate (DWP)[16], compensation of the chromatic dispersion by inserting an α-barium borate (BBO) crystal[17], coherent synthesis of THz pulses emitted from multiple filaments[18], tilting the β-BBO crystal to reduce the walk-off effect, which takes place during the SH generation[19], and changing the gas species[10]. Nevertheless, the highest THz pulse energy obtained by Ti:sapphire femtosecond laser filamentation so far is approximately 31 μJ, which is obtained by focusing terawatt, two-color laser pulses in air with a cylindrical lens[20]. The corresponding conversion efficiency is approximately 0.07%. Much work has been done in THz radiation generation by two-color (800 nm and 400 nm) field filamentation in argon gas[10,21,22]. So far, the THz energy conversion efficiency can reach up to 0.12% at 0.08 atm with the help of vacuum apparatus[22].

In the present work, an optical setup for generating THz pulses by femtosecond laser filament was carefully designed to realize a precise overlapping of two-color laser pulses both spatially and temporally. By using a commercial Ti:sapphire laser with a pulse energy of 6 mJ at 1 kHz repetition rate, the maximum output THz pulse energy reached 21 μJ in argon gas. The corresponding conversion efficiency exceeded 0.35%.

Experimental setup and results

Figure 1 illustrates the schematic representation of our experiments. During the experiments, a Ti:sapphire femtosecond laser amplifier (Legend, Coherent Inc.), which delivered 50 fs pulses with a central wavelength of 800 nm and a single-pulse energy up to 6 mJ at 1 kHz repetition rate, was employed. The horizontally polarized fundamental wave (FW) first passed through an air-spaced zero-order half-wave plate (HWP) and then was focused into a gas cell by a plano-convex lens (f = 300 mm). The focused femtosecond laser was frequency-doubled by a 107-μm-thick β-BBO crystal with type I phase matching. An 88-μm-thick α-BBO was used to compensate the time delay between the FW and SH pulses. The α-BBO was tilted to further achieve a precise spatial overlap of the two beams in Fig. 1. It should be noted that calcite retardation plates[23,24] and quartz wedges[25] can also be used for retardation compensation and relative phase control. In addition, compared with the experimental scheme using the dichroic mirror to separate the first and second harmonic beams and control the time delay between them by the optical delay line[26], the experimental setup used in this paper has smaller mechanical vibrations, higher laser energy utilization, more compact equipment, and better use of space. In addition, a DWP was set to make the polarizations of the FW and SH pulses parallel. The DWP worked as an HWP at 800 nm but as a full-wave plate at 400 nm. Furthermore, the mounted DWP was also installed as the entrance window of the gas cell. In the gas cell, the polarization of the fundamental laser beam is always parallel to the polarization of the second harmonic laser beam[27]. The pressure in the gas cell was maintained at 1 atm. A 2 mm thick Teflon plate was installed at the exiting window to block the FW and SH pulses, while transmitting THz radiation for detection.

An off-axis parabolic mirror (1st OAP) with a diameter of 2 inches and a focal length of 4 inches was used to collect and collimate the forward-propagation THz pulses emitted by the filament. The collimated THz pulses were focused by the 2nd OAP into a Golay cell detector (GC-1P, Tydex Inc.) equipped with a 6 mm diameter high-density polyethylene input window to measure the THz energy. It should be noted that in order to detect the THz pulses using the Golay cell, the femtosecond laser beam output from the laser systems is modulated by a chopper with a frequency of 15 Hz. Six pieces of 2 mm thick Teflon plates and one piece of 400 μm thick high-resistance silicon wafer were placed between 1st OAP and 2nd OAP. Another 400 μm thick high-resistance silicon wafer[28] and a THz low-pass filter with the cut-off frequency of 3.2 THz (LPF3.2-24, Tydex Inc.) were placed in front of the Golay cell window to completely filter out femtosecond laser and stray light. These measures guarantee only the THz radiation can be detected by the Golay cell. Due to the attenuation induced by the Teflon plates, high-resistance silicon wafers, the low-pass filter and the water vapor in air, the THz pulse power incident on the Golay cell is not larger than the upper power limit of the detector. The THz pulse energy

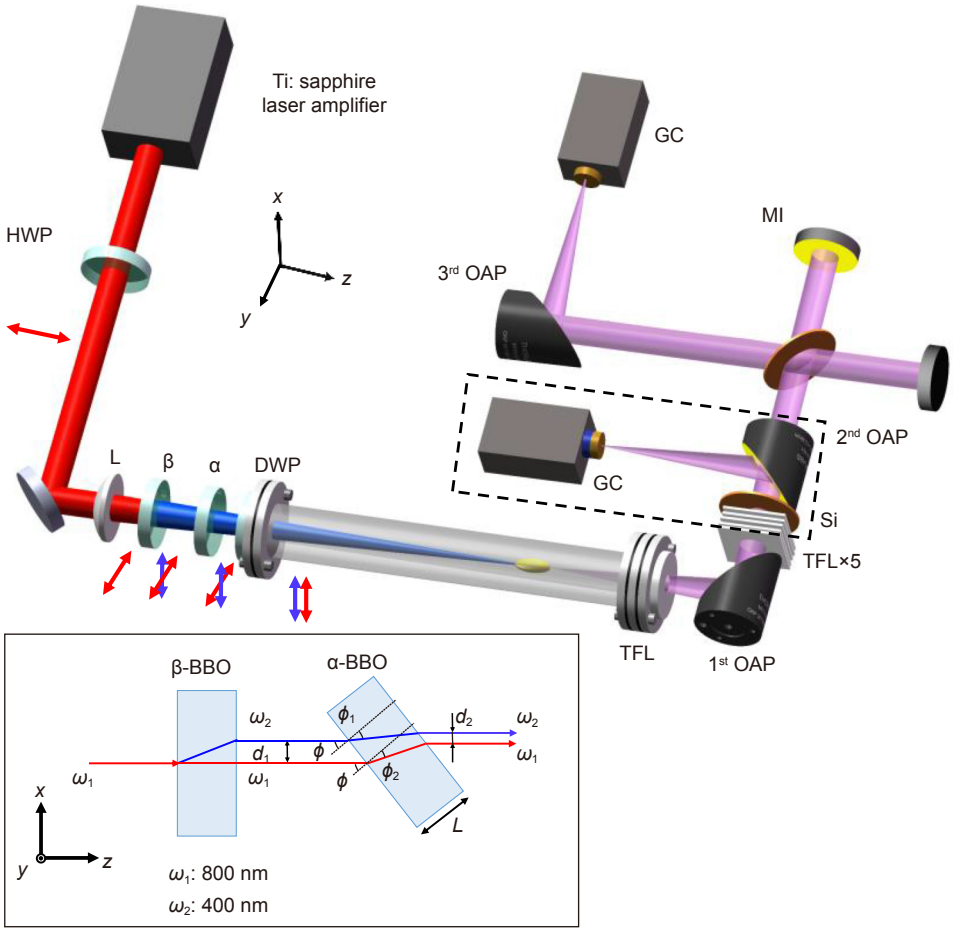

Fig. 1 | Experimental setup for high-energy THz pulse generation by filamentation in gases. The optical elements in the dashed frame need to be removed when measuring the THz autocorrelation curve. HWP: half-wave plate; L: lens; β: β-BBO; α: α-BBO; DWP: dual-wavelength plate; TFL: Teflon; OAP: 90° off-axis parabolic mirror; Si: silicon wafer; GC: Golay cell. Inset: tilting of α-BBO can further realize the precise spatial overlap of two beams.

generated by the dual-color field filamentation can be calculated according to the signal measured by the Golay cell.

Furthermore, the first order autocorrelation of the THz pulse can be measured using the Michelson interferometer when the apparatus in the dashed rectangular frame is removed from Fig. 1. The spectrum of the THz pulse can be obtained by Fourier transforming the autocorrelation trace.

We firstly measured the dependence of the THz pulse energy on the frequency chirp of the femtosecond laser pulse introduced by the compressor of the femtosecond laser amplifier, which is shown in Fig. 2. In Fig. 2, the THz pulse is generated in argon gas, the chirp parameter $C = (8\ln 2)\beta''\Delta z/\tau^2$ where β'' is the group velocity dispersion of the grating pair of the compressor, Δz is the change of the effective grating spacing, τ is the pulse duration of the chirp-free laser pulse. It is found that femtosecond laser pulses with a negative chirp of $C = 0.66$ can generate THz pulses with the largest pulse energy since the group delay dispersions of the transparent elements in the beam path are compensated in this case[29]. During

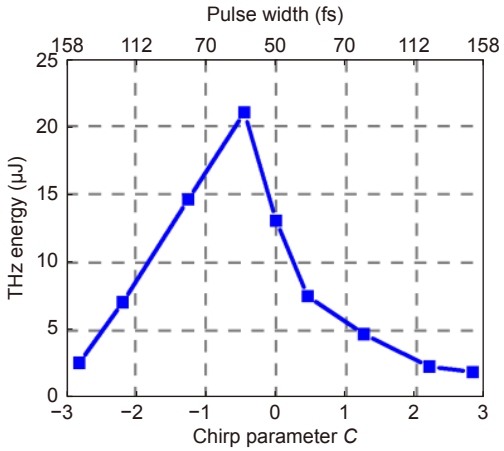

Fig. 2 | Pulse energy of THz radiation generated by femtosecond laser with different frequency chirps (bottom axis) and different pulse widths (top axis) in argon.

the following experiments, the chirp parameter C is set to be 0.66.

Figure 3 outlines the variation of the output THz pulse energy as functions of the pumping laser energy in different gases, namely, ambient air (black squares), nitrogen (red circles), and argon (blue triangles), and the solid lines are fitting lines of these experimental data. It is known that as the laser pulse energy increases, the length of the filament increases accordingly for small laser pulse energy, then gradually reaches an upper limit and stops increasing further[9,30]. Besides, it is also known that the THz pulse energy is proportional to the square of the filament length[31]. Therefore, the data points in Fig. 3(a) can be fitted using the analytical expression of $y = (Ax - B)/(C + \sqrt{Dx - E})^2$ derived from the relation between the THz pulse energy and the filament length. It should be noted that when the laser pulse energy is 6 mJ, the filament lengths, i.e. the full widths at half maximum of the filament fluorescence distribution along the laser propagation direction, are respectively 3 mm, 4.3 and 4.5 mm in Ar, N_2 and air. In the three cases, the THz pulse energy rapidly increases at a low laser energy. However, the outputs tend to saturate at 3.5, 2.8 and 2.2 mJ for air, nitrogen, and argon, respectively. Moreover, the highest THz pulse energy of 21 μJ was obtained experimentally in argon gas. The corresponding energy conversion efficiency is approximately 0.35%, and the maximum THz pulse energies in air and nitrogen are 6.8 and 8 μJ, respectively. The results agree with the previously reported observations, which could be attributed to the difference in the ionization rates of three gases[10]. It is worth emphasizing that to optimize the THz pulse energy, α-BBO was tilted during the experiments to compensate the walk-off effect during the SH generation process in β-BBO. For example, the measured THz pulse energies in argon are indicated in Fig. 3(b) as black squares as a function of the titling angle ϕ of α-BBO. The maximum energy of 21 μJ appears at ϕ = 32.5°. Furthermore, typical autocorrelation traces and corresponding spectra of the generation THz pulse in argon are demonstrated in Fig. 4. The obtained spectra cover a broad range up to 25 THz.

Discussion

Generally, from a microscopic view, the THz pulse generation inside a filament plasma mainly contributes to the transient photon current induced by femtosecond laser driving free electrons[1]. At low laser energies, the free electron density dramatically increases when the laser energy increases, because the ionization is a highly nonlinear process. However, when the laser peak power exceeds the critical power for self-focusing, the so-called intensity clamping effect takes place, which is induced by the balance between the optical Kerr self-focusing and plasma defocusing[32,33]. The critical power for self-focusing in air, nitrogen and argon are 3.5, 4.4 and 7.2 GW, respectively[34,35]. Consequently, the focused laser intensity does not significantly increase during a further increase of laser energy. Such a result is manifested as the saturation of the output THz pulse energy at high laser energies in Fig. 3(a). The fitting curves of the experimental data illustrated in Fig. 3(a) are indicated as solid

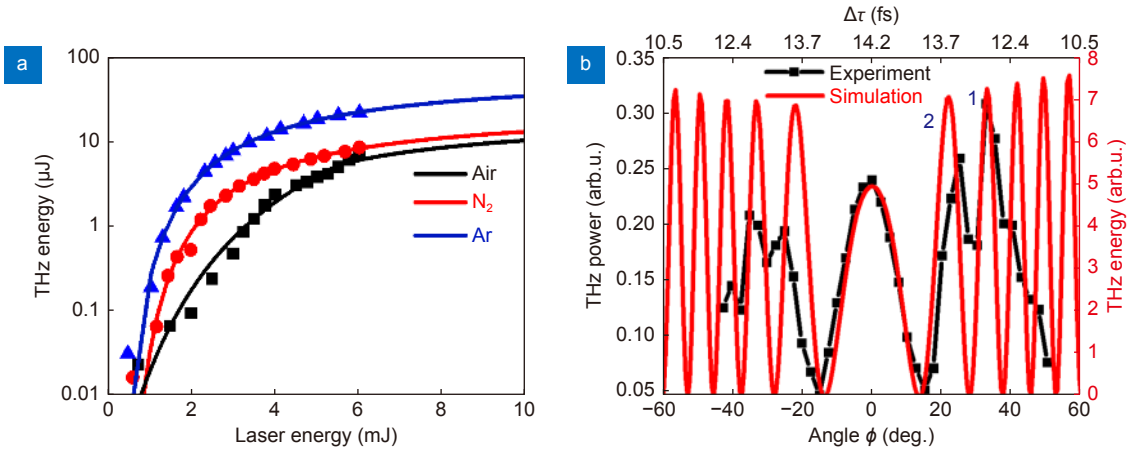

Fig. 3 | Variation of the output THz pulse energy as a function of (**a**) pumping laser energy in different gases and (**b**) tilting angle of α-BBO (bottom axis), i.e. the time delay between the fundamental and second harmonic laser beams (upper axis) in argon. In (a): black squares – ambient air, red circles – nitrogen, and blue triangles – argon; solid lines: data fitting curves. (b) black squares: experimental data; red line: numerical simulation results.

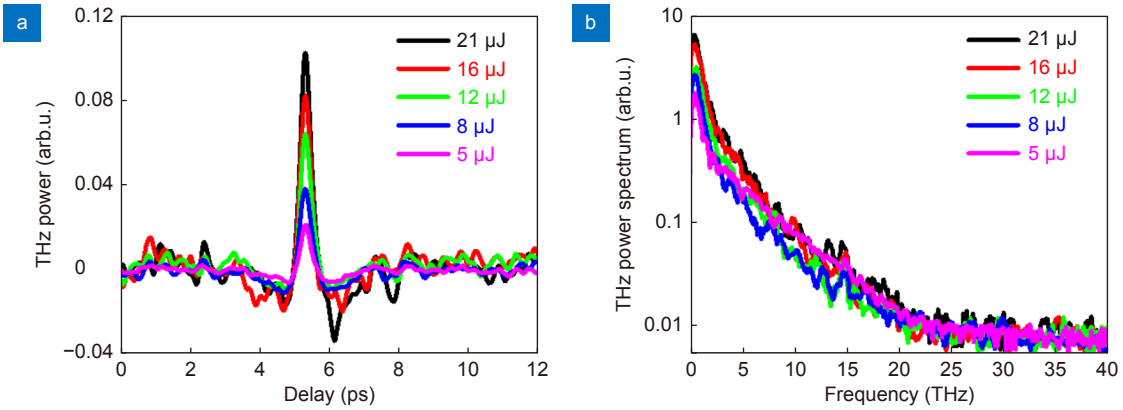

Fig. 4 | (**a**) Autocorrelation traces and (**b**) spectra of various energy THz pulses in argon.

lines. According to the fitting results, the THz pulse energy can be expected to be more than 30 μJ when the laser energy reaches 10 mJ. Table 1 compares the THz generation efficiency achieved in this paper with the reported highest THz generation efficiency of the two-color field filamentation (800 nm + 400 nm) in argon with different pressures.

Table 1 | Energy conversion efficiency Q_{THz} of THz pulse generated by the two-color field (800 nm + 400 nm) filamentation in argon gas.

λ (μm)	Pressure (Torr(1 Torr=133 Pa))	Q_{THz} (%)
0.8[10]	600	0.01
0.8[21]	700	0.015
0.8[22]	60	0.12
0.8 (this work)	760	0.35

α-BBO is mainly used to simultaneously compensate the temporal delay and the spatial walk-off distance between two beams. Table 2 lists the calculated temporal delay $\Delta\tau$ between two beams in our experiments when the sample cell is filled with argon. The calculations were performed based on the given group velocities in crystals, air, and argon[36].

In addition, the walk-off effect was investigated. Following the method described in our previous work[19], the detailed calculations show that due to the small focusing numerical aperture (NA) of 0.015 in Fig. 1, taking the focusing laser beam as a plane wave in calculating the walk-off distance and the temporal delay between the fundamental and second harmonic laser beams is reasonable. The system temporal delay and walk-off distance caused by tilting α-BBO can be expressed as:

$$d_2 = d_1 + (L\tan\phi_1 - L\tan\phi_2)\cos(\phi)\ , \tag{1}$$

$$\Delta\tau_3 = \frac{L}{\cos\phi_2 \cdot v_g(\omega_2)} + \frac{d_2\tan\phi - d_1\tan\phi}{c} - \frac{L}{\cos\phi_1 \cdot v_g(\omega_1)}\ , \tag{2}$$

$$\Delta\tau = \Delta\tau_1 + \Delta\tau_2 + \Delta\tau_3 + \Delta\tau_4 + \Delta\tau_5\ , \tag{3}$$

where ϕ , ϕ_1 and ϕ_2 denote the tilt angle of α-BBO, the refraction angles of 800 nm and 400 nm laser light incident on the α-BBO interface, respectively. L corresponds to the thickness of α-BBO. d_1 represents the estimated walk-off distance introduced by β-BBO. d_2 refers to the system walk-off distance after tilting α-BBO. c, $v_g(\omega_1)$ and $v_g(\omega_2)$ are the light speed in vacuum. The group velocities of 800 nm and 400 nm lasers in α-BBO, respectively. $\Delta\tau_1$, $\Delta\tau_2$, $\Delta\tau_3$, $\Delta\tau_4$, and $\Delta\tau_5$ point to the temporal delay of the two-color laser passing through β-BBO, air, α-BBO, DWP, and argon, respectively. $\Delta\tau$ denotes the resulted total temporal delay.

According to the photocurrent model[41], if the optical electric fields of 800 nm and 400 nm laser beams are expressed as $E = E_0\cos(\omega t)$ and $E = E_0\cos(2\omega t+\theta)$ respectively, the THz pulse with the largest pulse energy can be

Table 2 | Calculated temporal delay between two beams in the experiments.

Medium	Thickness (μm)	v_g (800 nm) (×10^8 m/s)	v_g (400 nm) (×10^8 m/s)	$\Delta\tau$ (fs)
β-BBO[37]	107±1	1.7809	1.7217	21.97
Air[38]	5×10^4	2.999587	2.999552	1.97
α-BBO[39](@ ϕ = 0°)	88±1	1.7774	1.8605	–22.1
DWP[40]	45±1	1.9247	1.8553	8.7
Argon[38]	5×10^4	2.999158	2.999092	3.67

generated for $\theta = \pi/2+k\pi$ (k is an integer). This case appears when the optical electric fields of 800 nm and 400 nm laser beams intersect with each other at t axis based on the photocurrent model[41] as shown in Fig. 5. It is also seen that if the time delay between the two-color laser beams changes by half of the optical cycle of 400 nm laser, i.e. 0.66 fs, the optical electric fields of 800 nm and 400 nm laser beams intersect with each other at t axis again. Therefore, the THz energy oscillation period is equal to half of the optical cycle of 400 nm laser beam, i.e. 0.66 fs, which agrees with Fig. 3(b).

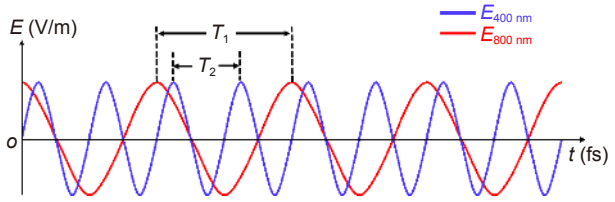

Fig. 5 | Schematic diagram of the electric fields of the two-color laser beams.

The tilting angle-dependent temporal delay (red solid line) and the walk-off distance (blue dashed line) between the two beams are illustrated in Fig. 6. If there is no tilting of α-BBO, the walk-off distance is approximately 7.3 μm. However, the walk-off distance reduced to 5.2 μm when $\phi = 32.5°$. In particular, the titling angle-dependent refractive index distribution was taken into account during the calculation of the results illustrated in Fig. 6. At the same time, $\Delta\tau$ changed from 14.2 fs to 13 fs when the tilting angle was rotated to 32.5°. The change of the α-BBO's tilting angle directly causes the change of the time delay between the fundamental and the second harmonic laser beams, thereby causing the change of the terahertz pulse energy. Using Eqs. (1–3), the time delay between the two-color laser beams can be calculated for each tilting angle as is shown in the top axis of Fig. 3(b). In Fig. 3(b), two oscillation peaks numbered by 1 and 2 exist for experimental data. These oscillation peaks have a similar period with those calculated by the photocurrent model (red solid curve). This condition explains the multiple maxima observed in Fig. 3(b) because the corresponding delays among the maxima are approximately 0.66 fs according to the results depicted in Fig. 6. It is also seen that when the α-BBO crystal is tilted, the time delay between the fundamental and second harmonic laser beams is identical for the positive and negative angles with identical absolute values. However, for the positive tilting angle of α-BBO, the spatial walk-off distance between the two-color laser beams is smaller than that with negative tilting angle, so the THz energy conversion efficiency is higher when the tilting angle of α-BBO is positive. Moreover, when the tilting angle is more than 40°, the laser beams would be partially clipped because of the limited crystal size. This case is manifested as the decrease of THz pulse energy at tilting angles larger than 40°. Nevertheless, the results were verified by a numerical simulation, which proved that further increase of the tilting angle of α-BBO would not enhance the maximum THz pulse energy significantly mainly because of the relatively long pulse duration (50 fs) used in our experiments.

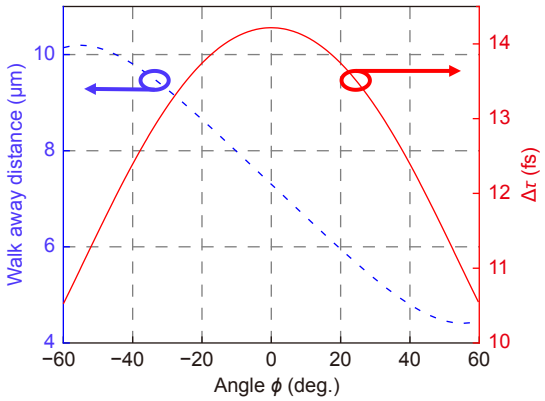

Fig. 6 | Temporal delay (red solid line) and walk-off distance (blue dashed line) between two beams with respect to the tilting angle of α-BBO in the case of argon.

Conclusions

In this work, an improved optical setup of THz pulse generation through femtosecond laser filament in gases was demonstrated. When a typical two-color laser scheme was implemented, the tilting of α-BBO was introduced to optimize the temporal delay and spatial walk-off between two beams. As a result, the maximum THz pulse energy of 21 μJ, which yields an energy conversion efficiency of 0.35%, was obtained in argon gas. The pumping laser energy was 6 mJ at 1 kHz repetition rate. In the future, the conversion efficiency can potentially be further enhanced through the implementation of additional methods, such as extending the laser wavelength to infrared,[14,42] using shorter pulses and perfectly designed compensating crystals. The gas pressure is also an important parameter that can improve the THz generation efficiency[21,43]. Therefore, generating strong THz pulse by femtosecond laser with a moderate pulse energy can be expected.

References

1. Zhang XC, Shkurinov A, Zhang Y. Extreme terahertz science. *Nat Photonics* **11**, 16–18 (2017).
2. Kampfrath T, Tanaka K, Nelson KA. Resonant and nonresonant control over matter and light by intense terahertz transients. *Nat Photonics* **7**, 680–690 (2013).
3. Fülöp JA, Ollmann Z, Lombosi C, Skrobol C, Klingebiel S et al. Efficient generation of THz pulses with 0.4 mJ energy. *Opt Express* **22**, 20155–20163 (2014).
4. Zhang BL, Ma ZZ, Ma JL, Wu XJ, Ouyang C et al. 1.4 - mJ high energy terahertz radiation from lithium niobates. *Laser Photonics Rev* **15**, 2000295 (2021).
5. Vicario C, Ovchinnikov AV, Ashitkov SI, Agranat MB, Fortov VE et al. Generation of 0.9-mJ THz pulses in DSTMS pumped by a Cr: Mg_2SiO_4 laser. *Opt Lett* **39**, 6632–6635 (2014).
6. Shalaby M, Hauri CP. Demonstration of a low-frequency three-dimensional terahertz bullet with extreme brightness. *Nat Commun* **6**, 5976 (2015).
7. Liao GQ, Li YT, Liu H, Scott GG, Neely D et al. Multimillijoule coherent terahertz bursts from picosecond laser-irradiated metal foils. *Proc Natl Acad Sci USA* **116**, 3994–3999 (2019).
8. Tian Y, Liu JS, Bai YF, Zhou SY, Sun HY et al. Femtosecond-laser-driven wire-guided helical undulator for intense terahertz radiation. *Nat Photonics* **11**, 242–246 (2017).
9. Roskos HG, Thomson MD, Kreß M, Löffler T. Broadband THz emission from gas plasmas induced by femtosecond optical pulses: from fundamentals to applications. *Laser Photonics Rev* **1**, 349–368 (2007).
10. Kim KY, Taylor AJ, Glownia JH, Rodriguez G. Coherent control of terahertz supercontinuum generation in ultrafast laser–gas interactions. *Nat Photonics* **2**, 605–609 (2008).
11. Meng FH, Cheng R, Deng C, Zhong ZY. Intracellular drug release nanosystems. *Mater Today* **15**, 436–442 (2012).
12. Andreeva VA, Kosareva OG, Panov NA, Shipilo DE, Solyankin PM et al. Ultrabroad terahertz spectrum generation from an air-based filament plasma. *Phys Rev Lett* **116**, 063902 (2016).
13. Matsubara E, Nagai M, Ashida M. Ultrabroadband coherent electric field from far infrared to 200 THz using air plasma induced by 10 fs pulses. *Appl Phys Lett* **101**, 011105 (2012).
14. Koulouklidis AD, Gollner C, Shumakova V, Fedorov VY, Pugžlys A et al. Observation of extremely efficient terahertz generation from mid-infrared two-color laser filaments. *Nat Commun* **11**, 292 (2020).
15. Clerici M, Peccianti M, Schmidt BE, Caspani L, Shalaby M et al. Wavelength scaling of terahertz generation by gas ionization. *Phys Rev Lett* **110**, 253901 (2013).
16. Oh TI, Yoo YJ, You YS, Kim KY. Generation of strong terahertz fields exceeding 8 MV/cm at 1 kHz and real-time beam profiling. *Appl Phys Lett* **105**, 041103 (2014).
17. Zhang ZL, Chen YP, Cui S, He F, Chen M et al. Manipulation of polarizations for broadband terahertz waves emitted from laser plasma filaments. *Nat Photonics* **12**, 554–559 (2018).
18. Zhao JY, Guo LJ, Chu W, Zeng B, Gao H et al. Simple method to enhance terahertz radiation from femtosecond laser filament array with a step phase plate. *Opt Lett* **40**, 3838–3841 (2015).
19. Su Q, Liu WW, Lu D, Qi PF, Kosareva O et al. Influence of the tilting angle of a BBO crystal on the terahertz radiation produced by a dual-color femtosecond laser. *IEEE Trans Terahertz Sci Technol* **9**, 669–674 (2019).
20. Kuk D, Yoo YJ, Rosenthal EW, Jhajj N, Milchberg HM et al. Generation of scalable terahertz radiation from cylindrically focused two-color laser pulses in air. *Appl Phys Lett* **108**, 121106 (2016).
21. Rodriguez G, Dakovski GL. Scaling behavior of ultrafast two-color terahertz generation in plasma gas targets: energy and pressure dependence. *Opt Express* **18**, 15130–15143 (2010).
22. Yoo YJ, Jang D, Kim KY. Highly enhanced terahertz conversion by two-color laser filamentation at low gas pressures. *Opt Express* **27**, 22663–22673 (2019).
23. Ushakov AA, Chizhov PA, Andreeva VA, Panov NA, Shipilo DE et al. Ring and unimodal angular-frequency distribution of THz emission from two-color femtosecond plasma spark. *Opt Express* **26**, 18202–18213 (2018).
24. Ushakov A, Chizhov P, Bukin V, Shipilo D, Panov N et al. Multiple filamentation effects on THz radiation pattern from laser plasma in air. *Photonics* **8**, 4 (2021).
25. Dai JM, Karpowicz N, Zhang XC. Coherent polarization control of terahertz waves generated from two-color laser-induced gas plasma. *Phys Rev Lett* **103**, 023001 (2009).
26. Kosareva O, Esaulkov M, Panov N, Andreeva V, Shipilo D et al. Polarization control of terahertz radiation from two-color femtosecond gas breakdown plasma. *Opt Lett* **43**, 90–93 (2018).
27. Dai HM, Liu JS. Terahertz emission dependence on the irradiating laser pulse width in generating terahertz waves from two-color laser-induced gas plasma. *J Mod Opt* **58**, 859–864 (2011).
28. Li JS, Li JR. Dielectric properties of silicon in terahertz wave region. *Microw Opt Technol Lett* **50**, 1143–1146 (2008).
29. Zhang Z, Panov N, Andreeva V et al. Optimum chirp for efficient terahertz generation from two-color femtosecond pulses in air. *Appl Phys Lett* **113**, 241103 (2018).
30. Marburger JH. Self-focusing: theory. *Prog Quantum Electron* **4**, 35–110 (1975).
31. You YS, Oh TI, Kim KY. Off-axis phase-matched terahertz emission from two-color laser-induced plasma filaments. *Phys Rev Lett* **109**, 183902 (2012).
32. Liu W, Petit S, Becker A, Aközbek N, Bowden CM et al. Intensity clamping of a femtosecond laser pulse in condensed matter. *Opt Commun* **202**, 189–197 (2002).
33. Liu WW. Intensity clamping during femtosecond laser filamentation. *Chin J Phys* **52**, 465–489 (2014).
34. Nibbering ETJ, Grillon G, Franco MA, Prade BS, Mysyrowicz A. Determination of the inertial contribution to the nonlinear refractive index of air, N_2, and O_2 by use of unfocused high-intensity femtosecond laser pulses. *J Opt Soc Am B* **14**, 650–660 (1997).
35. Nuter R, Skupin S, Bergé L. Chirp-induced dynamics of femtosecond filaments in air. *Opt Lett* **30**, 917–919 (2005).
36. Wang PQ. Group velocity of light in uniaxial crystals. *Appl Opt* **60**, 1987–1994 (2021).
37. Zhang DX, Kong YF, Zhang JY. Optical parametric properties of

532-nm-pumped beta-barium-borate near the infrared absorption edge. *Opt Commun* **184**, 485–491 (2000).

38. Zhang J, Lu ZH, Wang LJ. Precision refractive index measurements of air, N_2, O_2, Ar, and CO_2 with a frequency comb. *Appl Opt* **47**, 3143–3151 (2008).
39. https://cetest02.cn-bj.ufileos.com/100001_1911295109%2FBirefringent%20Crystals_%CE%B1-BBO.pdf.
40. Zhao S, Wu FQ. The study on dispersive equation and thermal refractive index coefficient of quartz crystal. *Acta Photonica Sin* **35**, 1183–1186 (2006).
41. Kim KY. Generation of coherent terahertz radiation in ultrafast laser-gas interactions. *Phys Plasmas* **16**, 056706 (2009).
42. Jang D, Schwartz RM, Woodbury D, Griff-McMahon J, Younis AH et al. Efficient terahertz and Brunel harmonic generation from air plasma via mid-infrared coherent control. *Optica* **6**, 1338–1341 (2019).
43. Solyankin PM, Nikolaeva IA, Angeluts AA, Shipilo DE, Minaev NV et al. THz generation from laser-induced breakdown in pressurized molecular gases: on the way to terahertz remote sensing of the atmospheres of Mars and Venus. *New J Phys* **22**, 013039 (2020).

Acknowledgements

National Natural Science Foundation of China (12061131010, 12074198), Russian Science Foundation (21-49-00023).

Author contributions

Z. Q. Yu, N. Zhang, W. W. Liu performed the measurements. J. X. Wang, Z. J. Dai and C. Gong provided help in result analysis and numerical simulation. L. Lin contributed in revision of this paper. W. W. Liu proposed the original idea and supervised the project.

Competing interests

The authors declare no competing financial interests.

Supplementary information

Supplementary information for this paper is available at https://doi.org/10.29026/oea.2022.210065